REPORT

NANOPHOTONICS

Revealing the subfemtosecond dynamics of orbital angular momentum in nanoplasmonic vortices

G. Spektor,[1] D. Kilbane,[2,3] A. K. Mahro,[2] B. Frank,[4] S. Ristok,[4] L. Gal,[1] P. Kahl,[5] D. Podbiel,[5] S. Mathias,[2,6] H. Giessen,[4]* F.-J. Meyer zu Heringdorf,[5]* M. Orenstein,[1]* M. Aeschlimann[2]*

The ability of light to carry and deliver orbital angular momentum (OAM) in the form of optical vortices has attracted much interest. The physical properties of light with a helical wavefront can be confined onto two-dimensional surfaces with subwavelength dimensions in the form of plasmonic vortices, opening avenues for thus far unknown light-matter interactions. Because of their extreme rotational velocity, the ultrafast dynamics of such vortices remained unexplored. Here we show the detailed spatiotemporal evolution of nanovortices using time-resolved two-photon photoemission electron microscopy. We observe both long- and short-range plasmonic vortices confined to deep subwavelength dimensions on the scale of 100 nanometers with nanometer spatial resolution and subfemtosecond time-step resolution. Finally, by measuring the angular velocity of the vortex, we directly extract the OAM magnitude of light.

Since the theoretical work of Poynting (*1*) in 1909 and the experiments by Beth (*2*, *3*) from 1935–1936, it has been known that light can carry angular momentum. For almost a century, it was entirely attributed to the coordinate-independent "spin" angular momentum ($\pm\hbar$ per photon, where $\hbar$ is Planck's constant h divided by 2π), associated with right- and left-circularly polarized light. Following the pioneering work by Allen *et al.* (*4*), it was realized that light can also carry orbital angular momentum (OAM) in the circulating Poynting flow associated with helical wavefronts of an optical vortex field. A number of demonstrations and applications of light beams with OAM have been brought forward (*5*). They range from optical data storage (*6*, *7*) and optical tweezers (*8*) to quantum cryptography (*9*), communication (*10*–*12*), and astronomy (*13*), among others.

Recently, plasmonics has entered the field of OAM (*14*–*18*). Surface plasmon polaritons (SPPs) are electromagnetic waves bound to interfaces related to the collective oscillations of nearly free electrons in the conduction band (*19*, *20*). To control these waves, nanostructured metal surfaces were introduced as spatial light sources, generating structured optical fields in the near and far field (*21*–*23*).

Particularly, SPPs have the potential of confining fields that carry OAM to subwavelength dimensions. Archimedean spirals (*14*) and related nanostructures (*24*–*27*) were demonstrated to generate and control OAM-carrying plasmonic vortices under different illuminations. These advances provided many insights (*28*–*31*) into the nature of OAM, opening the door toward several exciting applications (*32*, *33*). Yet, to date, the actual dynamics of the formation of field patterns that carry OAM and their ultrafast revolution have remained unseen.

Here we experimentally reveal and measure the spatiotemporal dynamics of the formation of plasmonic vortices and their dressing by OAM. We image the evolution with subfemtosecond time steps Δt on nanometer spatial scales using time-resolved two-photon photoemission electron microscopy (TR-PEEM) (*34*). Furthermore, we confine the nanovortices to deep subwavelength scales of about $\lambda_{spp}/4$. The measured short-range SPP wavelength is 180 nm at vacuum wavelength of $\lambda_0 = 800$ nm. We examine the detailed origin of the field pattern formation, comparing our measurements with theoretical predictions. By measuring the angular velocity of the plasmonic nanovortices, we provide direct access to the value of the angular momentum of light. Our work also provides the direct recording of vortex fields rotating at optical frequencies (Fig. 1) and is of fundamental importance for the understanding of the dynamics of OAM generation, evolution, and possible coupling to associated atomic, molecular, and solid-state degrees of freedom.

A plasmonic vortex is generated when a protrusion or a slit in a metallic plate—for example, in the shape of an Archimedean spiral—is illuminated with circularly polarized light (*15*). The radius of a spiral of geometrical order m is given by $r = r_0 + m\lambda_{spp}\theta/2\pi$ (Fig. 2, A and B), where λ_{spp} is the SPP wavelength and θ is the azimuthal coordinate. When illuminated, the slit edges provide the necessary momentum to excite SPPs on the interface that propagate toward the interior of the spiral. The azimuthally varying radius of the two-dimensional (2D) slit profile provides a varying propagation phase to the SPPs excited along the profile. This geometrical phase together with the angular momentum carried by the impinging illumination ultimately determines the amount of OAM of the excited plasmonic vortex to be formed, which is related to the topological charge of the vortex. When the impinging illumination is circularly polarized, carrying photonic spin angular momentum through helicity $\pm\hbar$, its translation to an additional unit of plasmonic OAM is sometimes termed "spin-orbit coupling" but more accurately is rather a spin-to-OAM transformation process.

Exciting high-order vortices requires spirals with high m, as depicted in Fig. 2B. This is problematic because of the large extent of the spiraling wing, which is a source for azimuthally varying losses that deteriorate the performance. To mitigate this, we used a plasmonic vortex generator (*24*) of geometrical order m that utilizes the 2π periodicity of the SPP propagation phase by segmenting an Archimedean spiral of order m into m segments of the form $r_m(\theta) = r_i + \lambda_{spp}\cdot\mathrm{mod}(m\theta, 2\pi)/2\pi$ (Fig. 2C).

The time-averaged vortex field intensity has already been retrieved by techniques such as near-field scanning optical microscopy (*14*, *24*, *27*), resolving the radial field dependence. This dependence can be approximated as a Bessel function J of order l, $J_l(k_{spp}r)$, where k_{spp} is the plasmonic wave number, r is the radial coordinate, and l is directly related to the OAM magnitude of the vortex field (Fig. 2D and supplementary materials). Complementarily interferometric techniques also provided the steady-state azimuthal $e^{jl\theta}$ phase dependence of near- (*27*) and far-field (*5*, *35*) optical vortices (where $j = \sqrt{-1}$).

We fabricate the plasmonic vortex generators on atomically flat, single crystalline gold flakes that were grown on a silicon substrate. In such structures, we expect two different plasmonic modes to be supported (Fig. 2E). Long-range SPPs (shown in blue in Fig. 2E) are predominantly localized at the gold-vacuum interface and have a wavelength of $\lambda_{spp,long} \sim 780$ nm, only slightly shorter than that of the excitation source with $\lambda_0 = 800$ nm. The short-range SPPs (shown in red in Fig. 2E) are predominantly confined to the gold-silicon interface and have a considerably shorter wavelength, reaching down to

[1]Department of Electrical Engineering, Technion–Israel Institute of Technology, 32000 Haifa, Israel. [2]Department of Physics and State Research Center for Optics and Materials Sciences (OPTIMAS), University of Kaiserslautern, Erwin Schroedinger Strasse 46, 67663 Kaiserslautern, Germany. [3]School of Physics, University College Dublin, Belfield, Dublin 4, Ireland. [4]4th Physics Institute and Stuttgart Center of Photonics Engineering (SCoPE), University of Stuttgart, D-70569 Stuttgart, Germany. [5]Faculty of Physics and Center for Nanointegration Duisburg–Essen (CENIDE), University of Duisburg–Essen, Lotharstrasse 1-21, 47057 Duisburg, Germany. [6]I. Physikalisches Institut, Georg-August–Universität Göttingen, Friedrich-Hund-Platz 1, 37077 Göttingen, Germany.
***Corresponding author. Email: h.giessen@pi4.uni-stuttgart.de (H.G.); meyerzh@uni-due.de (F.-J.M.z.H.); meiro@ee.technion.ac.il (M.O.); ma@physik.uni-kl.de (M.A.)**

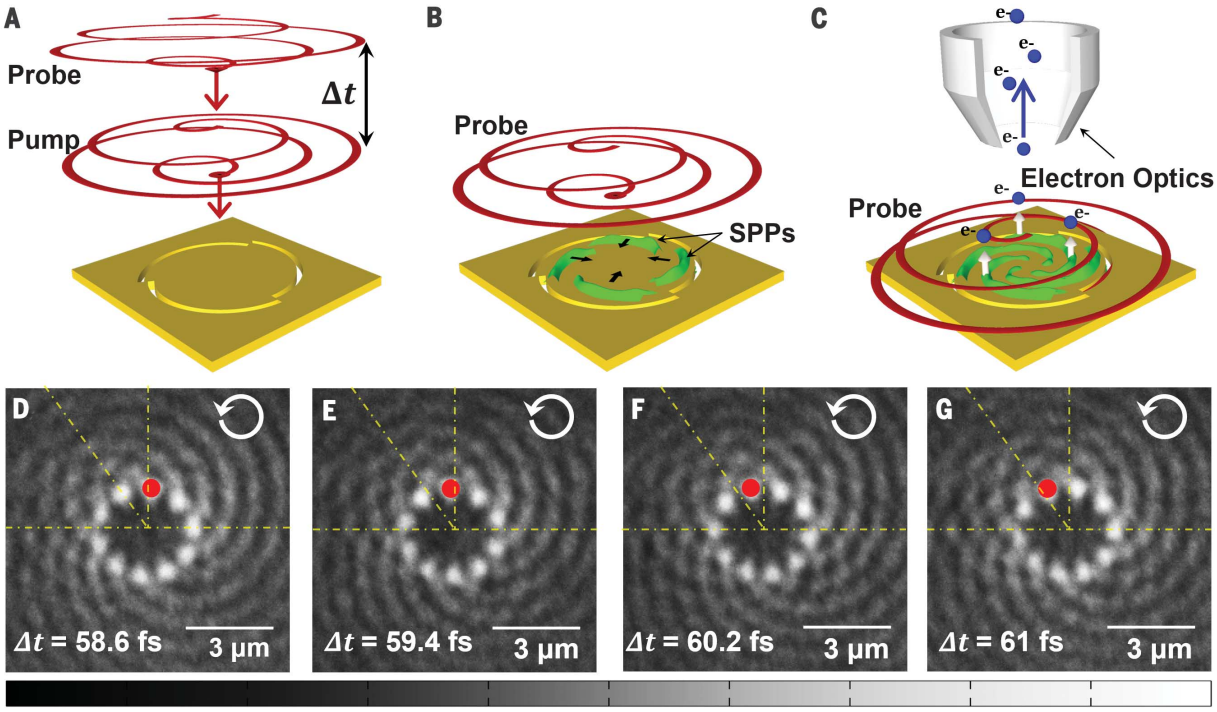

Fig. 1. Experimental concept and direct OAM extraction results. (**A** to **C**) Schematic experimental methodology. (A) Two circularly polarized ultrashort pulses with temporal separation Δt are launched at a plasmonic vortex–generating sample. (B) The pump pulse launches SPPs at the structure edges on the sample. (C) The probe pulse interferes with the propagating SPPs and liberates photoelectrons in a two-photon photoemission process, which are then imaged with the PEEM setup. Experimental TR-PEEM snapshot sequence (**D** to **G**) of the rotating field of a plasmonic vortex in the revolution stage within a single optical cycle of ~2.67 fs (movie S2). The 10 bright lobes evident in the measurement are related to the magnitude of OAM of the field. The red dot follows a specific lobe as it rotates around the center. The yellow dashed-dotted lines serve as reference frames to emphasize the rotation. The angle between the upper two yellow lines is 36°, corresponding to $2\pi/10$ rads.

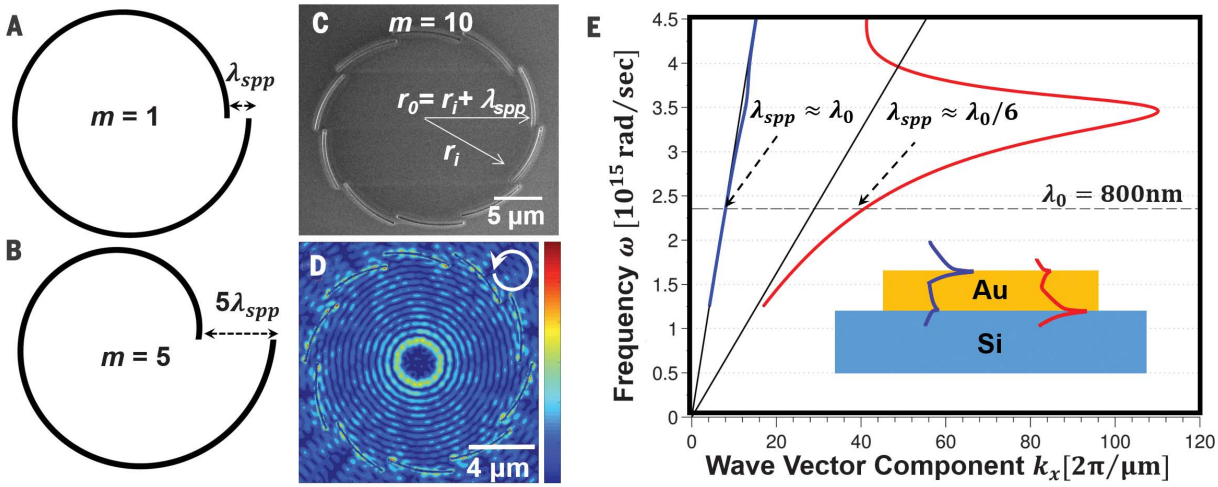

Fig. 2. Structure scheme and fabrication details. (**A**) Archimedean spiral slits of order $m = 1$ and (**B**) $m = 5$, demonstrating the azimuthal difference between different OAM-generating structures. (**C**) Scanning electron microscope image of a plasmonic vortex generator with geometrical order $m = 10$ milled into a gold layer. (**D**) Simulation of a steady-state, time-averaged, vortex field intensity created by the $m = 10$ structure upon right-handed circularly polarized illumination (white arrow). (**E**) Long-range (blue) and short-range (red) SPP dispersion curves. The inset depicts the long- and short-range SPPs formed on air-gold-silicon interface with a 20-nm gold slab. The gray solid lines are the light lines in air and silicon.

$\lambda_{spp,short}$ ~ 120 nm depending on the thickness of the gold layer, due to the high refractive index of silicon and their more plasmonic nature. When the gold layer thickness is below 30 to 40 nm, both modes can be excited and measured from the top, and both are investigated within this work.

In our time-resolved photoemission experiment, a circularly polarized ultrashort pulse (<23 fs) of central wavelength 800 nm is divided into two identical pulses in an actively stabilized Mach-Zehnder interferometer (*36*), providing subfemtosecond sampling time steps. Both pulses are

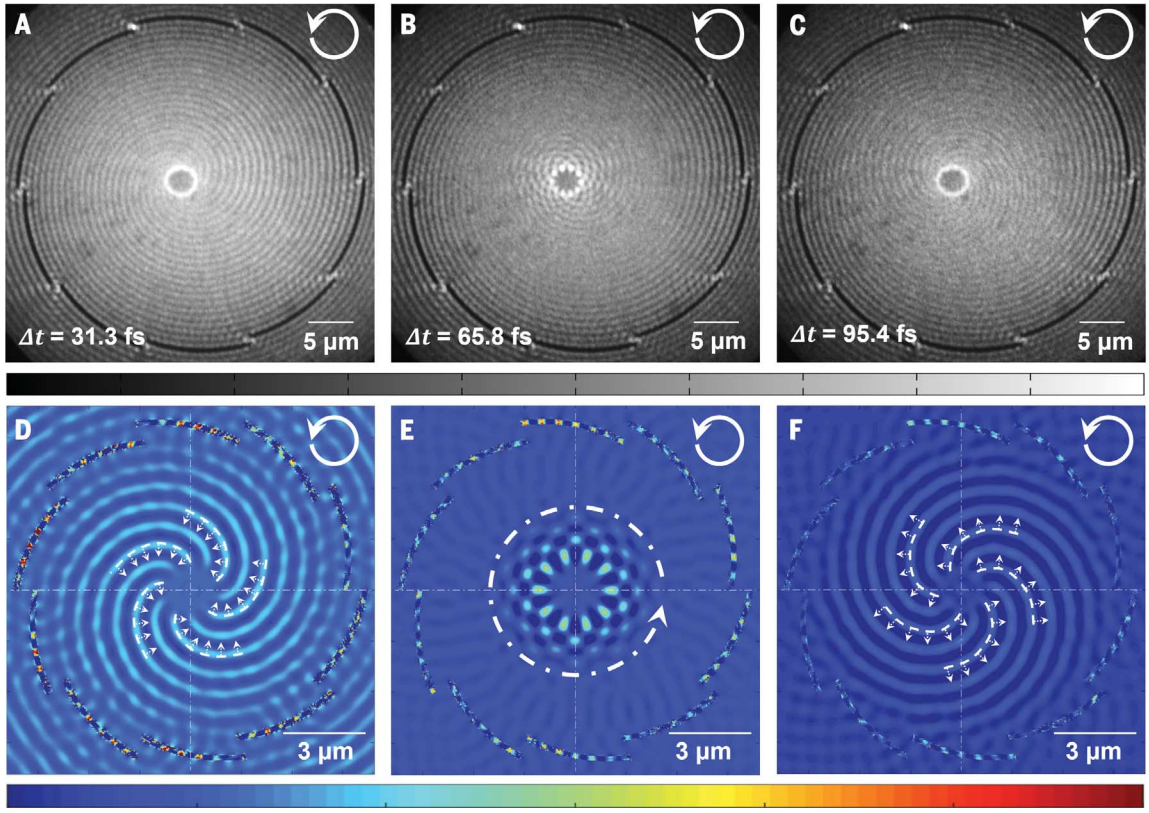

Fig. 3. Stages of vortex evolution—experiment and modeling. (**A** to **C**) Experimental TR-PEEM snapshot sequence from a plasmonic-vortex generator with m = 10 upon right-handed circularly polarized light illumination (indicated by the solid white arrows in the upper right). Showing the formation (A), revolution (B), and decay (C) stages of a plasmonic vortex at specific pump-probe time delays Δt. Modeling of the TR-PEEM signal (**D** to **F**), illustrating the corresponding stages. The small dashed arrows depict the propagation of the vortex wavefronts in each stage. The handedness of the spiraling wavefronts is reversed between the formation [(A) and (D)] and decay [(C) and (F)] stages. The white dashed arrow in (E) indicates the revolution direction of the vortex pattern (movies S1 and S2).

directed toward a structured gold sample at normal incidence (Fig. 1A). First, the pump pulse excites SPPs from the engraved edges on a gold surface (Fig. 1B). Second, the probe pulse impinges on the sample at subsequent time delays ($\Delta t > 0$ fs), interferes with the propagating SPPs, and liberates photoelectrons in a two-photon photoemission process (Fig. 1C). The emitted photoelectrons are then accelerated and focused by the electron optical lens system of the electron microscope (Fig. 1G), providing imaging with <30-nm spatial resolution. Recording images of the electron emission pattern at consecutive time steps Δt allows us to obtain suboptical-cycle time-resolved snapshots of the SPP electromagnetic fields as they propagate (Figs. 1, 3, and 4). In this way, we capture the ultrafast spatiotemporal dynamics of plasmonic vortices in a streakinglike fashion.

Here we measure and record the actual SPP wavefronts as they dynamically evolve from the boundaries to form a plasmonic vortex—namely, we are able to track in real time the formation, revolution, and decay of the OAM of plasmons. The plasmons are excited by a plasmon vortex generator of order m = 10 on a gold-vacuum interface with a plasmonic wavelength of λ_{spp} ~ 780 nm. We identify three stages in the lifetime of the vortex: the formation, revolution, and decay. The initial spin-orbit conversion of the vortex is due to the annihilation of the photons during the launching of SPPs from the boundaries of the Archimedean structure, forming converging spiraling wavefront threads (Fig. 3, A to D). This is followed by the concentration of the SPPs into the central region, where inward and outward counterpropagating SPPs interfere to form the radially standing but azimuthally rotating vortex field. This completes, by interference, the spin-to-OAM conversion process (Fig. 3, B to E). At this stage, we note the appearance of 10 rotating lobes, corresponding to the 10 azimuthal wavefronts of the steady-state $e^{10j\theta}$ phase of the vortex. It should be emphasized that the appearance of the rotating lobes is only observable within a time-resolved measurement in the subfemtosecond time domain. Otherwise, the lobes are smeared out to result in a time-averaged concentric-ring pattern with the dependence $J_{10}(k_{spp}r)$ (Fig. 2D).

In the final stage, namely the decay of the vortex, it dissolves (Fig. 3, C and F), forming outward-propagating spiraling wavefronts. Notably, this decay stage is characterized by a flip in the handedness of the spiraling wavefronts as compared to the formation stage (Fig. 3, A and D, and Fig. 3, C and F).

Several details of this observation include that the PEEM pattern in the vicinity of the cut-out nanoslits shows practically no dynamics within the formation phase of the vortex because it is predominantly the result of self-probing, which is photoemission of the probe (pump) pulse interference with the SPPs it generates (*34*). The radial extent of this static pattern is directly related to the pump and the probe pulse width (~23 fs), which amounts to r_{static} ~ 7 μm from the perimeter of the structure. The plasmonic vortex generator in Fig. 3 has an internal radius of r_i = 18 μm (Fig. 2C), asserting that for radii below $r_i - r_{static}$ ~ 11 μm, the signal is dominated by the desired dynamic photoemission emanated by the interference of the probe pulse with the pump-generated SPPs. In addition, the central region of the vortex generator features a static bright ring throughout the whole measurement as an additional static pattern. The generator concentrates SPPs from the perimeter toward the central region, there providing sufficient intensity of the plasmonic field for probe-independent plasmoemission (*37*) to occur regardless of the delay Δt (fig. S3).

Our experimental observations are supported by detailed modeling of the TR-PEEM signal. Figure 3, D to F, depicts the contribution to the PEEM signal of the expected dynamics resulting solely from the pump-excited SPPs sampled by the probe pulse. The exclusion of other photoemission contributions (e.g., the static pattern) from the model allows us to clearly identify the lifetime phases of the SPP vortex and interpret the obtained experimental results of the dynamic behavior of the plasmonic spin-orbit conversion.

The measurement of the angular velocity of the vortex rotation (ω_R) is indeed a direct measure of its integral angular momentum magnitude with the relation OAM per photon = $\hbar\omega/\omega_R$, where

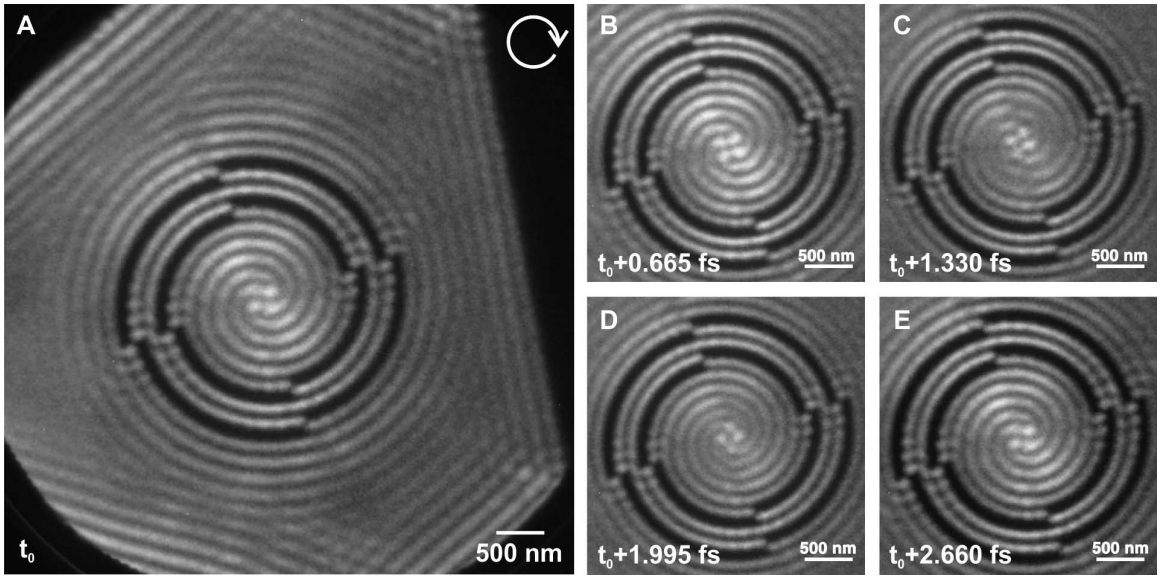

Fig. 4. Short-range plasmonic vortex. (**A**) Experimental TR-PEEM snapshots of short-range SPPs on a plasmonic-vortex generator of order m = 4. Short-range SPPs are excited at the edges of the structure and propagate to the center, where they form a rotating four-lobe pattern. The four images (**B** to **E**) are snapshots at four different time steps (0.665 fs apart), completing one full optical cycle (movie S3). The scale bars in images (B) to (E) are 500 nm, one order of magnitude smaller than in the images in Fig. 3.

ω is the light angular frequency. Concentrating on the second stage of the vortex evolution, where the vortex is fully evolved and predominantly only rotating, the series of suboptical-cycle snapshots in Fig. 1, D to G, clearly reveals the revolution of the SPP fields capturing the rotation of the fields around the center. We can clearly measure the dynamic pattern of 10 lobes encircling the dark center of the vortex. These lobes correspond to the azimuthal wavefronts of the vortex and were measured to exhibit angular velocity of 2π/10 rads per optical cycle corresponding to 10 units of angular momentum.

The measurement sequence depicted in Fig. 1, D to G, is taken starting 58.6 fs after the launching of the SPPs by the pump pulse. This time delay corresponds to SPPs propagating a distance of ~17.5 μm away from the perimeter to within the dynamic region. In the recorded time sequence, the pump-excited SPPs have already reached the central region from all locations on the perimeter and begin to propagate back toward the perimeter. Thus, the central pattern consists of the interference of inward and outward counterpropagating SPPs, and, therefore, the azimuthal dynamics can be approximated at this time interval by $\cos(l\theta - \omega t)$ without any radial motion, thus corroborating the observed experimental behavior as a function of the OAM magnitude l. The complete TR-PEEM movies, with 100-as (attosecond) time steps, are presented in the supplementary materials.

To generate truly deep subwavelength vortices, it is necessary to investigate short-range surface plasmons at the silicon-gold interface. We therefore discuss the dynamical behavior of these short-range plasmons, which form much more confined vortices, with typical spatial extent of tens of nanometers. To achieve this goal, we fabricated monocrystalline gold flakes electrochemically grown on a silicon substrate. The ~20-nm thin flakes support both long- and short-range SPPs (Fig. 2E), with the latter arising predominantly from the silicon-gold interface. We fabricated a double-slit plasmonic vortex–generator configuration, where the spacing of the concentric slits is half the long-range SPP wavelength (Fig. 4A). Thus, the long-range SPPs destructively interfere, and effectively are not excited, allowing the excitation of only the short-range SPPs (fig. S1). The measured short-range SPPs have a wavelength of λ_{spp} = 180 nm, which is the expected value considering the presence of a thin native-oxide layer on the silicon, reducing the effective refractive index (fig. S1). This results in a fourfold wavelength shortening compared to the 800-nm excitation wavelength. The sample was measured using a different PEEM setup (fig. S2 and supplementary methods) featuring ~15-fs pulses centered at the same 800-nm wavelength.

Figure 4 depicts the dynamics of a short-range plasmonic vortex within a plasmonic vortex generator of geometrical order m = 4 with r_i = 1 μm. As in the long-range SPP case, the measured pattern features static and dynamic regions. Because of the fourfold reduction of the phase velocity of the short-range SPPs, compared to the free-space propagation, the spatial extent of the static pattern is substantially shorter and comprises a static pattern radius of r_{static} ~ 600 nm toward the interior of the lens. The dynamic region of the vortex field shows four lobes that revolve around the center with a velocity of 2π/4 rads per optical cycle. Starting at t_0, a given lobe completes a π/2-rad revolution around the center of the vortex in 0.665-fs steps, illustrating the OAM of the short-range SPPs (movie S3).

Our observation and investigation on an ultrafast subfemtosecond time scale and nanometer lateral scale offer progress toward a better understanding and manipulation of the angular momentum degree of freedom of nanoplasmonic fields. The study reveals the nature of the plasmonic OAM and vortex formation and elucidate the process of light spin–to–plasmonic orbit transformation. Furthermore, these observations open new avenues for designing and directly measuring exciting applications of OAM in the nanoworld. Highly localized and surface-confined plasmonic vortices may become an important investigation tool for studying 2D materials with material angular momentum degrees of freedom such as topological insulators and thin-film magnetic and magneto-optic materials, as well as spintronic and valleytronic media. Additional applications may include enantiomer discrimination, realizations of higher-order qubits for chip-size quantum information, the rotation of nanoparticles in plasmonic tweezers (*33*, *38*), and the potential for dark-field nanofluorescent microscopic imaging. Finally, reducing the size of the vortex toward dimensions compatible with molecular wave functions may lead toward nondipolar transitions in quantum dots and molecules.

REFERENCES AND NOTES

1. J. Poynting, *Proc. R. Soc. London A Contain. Pap. Math. Phys. Character* **82**, 560–567 (1909).
2. R. A. Beth, *Phys. Rev.* **50**, 115–125 (1936).
3. R. A. Beth, *Phys. Rev.* **48**, 471 (1935).
4. L. Allen, M. W. Beijersbergen, R. J. Spreeuw J. P. Woerdman, *Phys. Rev. A* **45**, 8185–8189 (1992).
5. D. L. Andrews, M. Babiker, *The Angular Momentum of Light* (Cambridge Univ., 2012).
6. A. Nicolas *et al.*, *Nat. Photonics* **8**, 234–238 (2014).
7. D.-S. Ding, Z.-Y. Zhou, B.-S. Shi, G.-C. Guo, *Nat. Commun.* **4**, 2527 (2013).
8. M. Padgett, R. Bowman, *Nat. Photonics* **5**, 343–348 (2011).
9. G. Vallone *et al.*, *Phys. Rev. Lett.* **113**, 060503 (2014).
10. N. Bozinovic *et al.*, *Science* **340**, 1545–1548 (2013).
11. J. Wang *et al.*, *Nat. Photonics* **6**, 488–496 (2012).
12. G. Gibson *et al.*, *Opt. Express* **12**, 5448–5456 (2004).
13. F. Tamburini, B. Thidé, G. Molina-Terriza, G. Anzolin, *Nat. Phys.* **7**, 195–197 (2011).
14. Y. Gorodetski, A. Niv, V. Kleiner, E. Hasman, *Phys. Rev. Lett.* **101**, 043903 (2008).
15. Y. Gorodetski, N. Shitrit, I. Bretner, V. Kleiner, E. Hasman, *Nano Lett.* **9**, 3016–3019 (2009).
16. N. Shitrit, I. Bretner, Y. Gorodetski, V. Kleiner, E. Hasman, *Nano Lett.* **11**, 2038–2042 (2011).

17. G. Spektor, A. David, G. Bartal, M. Orenstein, A. Hayat, *Opt. Express* **23**, 32759–32765 (2015).
18. E. Karimi *et al*., *Light Sci. Appl.* **3**, e167 (2014).
19. H. Raether, *Surface Plasmons on Smooth Surfaces* (Springer, 1988).
20. S. A. Maier, *Plasmonics: Fundamentals and Applications* (Springer, 2007).
21. W. L. Barnes, A. Dereux, T. W. Ebbesen, *Nature* **424**, 824–830 (2003).
22. P. Genevet, F. Capasso, *Rep. Prog. Phys.* **78**, 024401 (2015).
23. G. M. Lerman, A. Yanai, U. Levy, *Nano Lett.* **9**, 2139–2143 (2009).
24. H. Kim *et al*., *Nano Lett.* **10**, 529–536 (2010).
25. G. Spektor, A. David, B. Gjonaj, G. Bartal, M. Orenstein, *Nano Lett.* **15**, 5739–5743 (2015).
26. G. Spektor *et al*., *Opt. Express* **24**, 2436–2442 (2016).
27. A. David, B. Gjonaj, Y. Blau, S. Dolev, G. Bartal, *Optica* **2**, 1045–1048 (2015).
28. K. Bliokh, F. J. Rodriguez-Fortuno, F. Nori, A. V. Zayats, *Nat. Photonics* **9**, 796–808 (2015).
29. A. M. Yao, M. J. Padgett, *Adv. Opt. Photonics* **3**, 161–204 (2011).
30. K. Y. Bliokh, A. Niv, V. Kleiner, E. Hasman, *Nat. Photonics* **2**, 748–753 (2008).
31. K. Y. Bliokh, A. Y. Bekshaev, F. Nori, *Nat. Commun.* **5**, 3300 (2014).
32. F. Cardano, L. Marrucci, *Nat. Photonics* **9**, 776–778 (2015).
33. W.-Y. Tsai, J.-S. Huang, C.-B. Huang, *Nano Lett.* **14**, 547–552 (2014).
34. P. Kahl *et al*., *Plasmonics* **9**, 1401–1407 (2014).
35. M. Mirhosseini *et al*., *Opt. Express* **21**, 30196–30203 (2013).
36. M. U. Wehner, M. H. Ulm, M. Wegener, *Opt. Lett.* **22**, 1455–1457 (1997).
37. D. Podbiel, P. Kahl, F.-J. Meyer zu Heringdorf, *Appl. Phys. B* **122**, 90 (2016).
38. M. L. Juan, M. Righini, R. Quidant, *Nat. Photonics* **5**, 349–356 (2011).

ACKNOWLEDGMENTS

This research was supported partially by the Israeli Centers of Research Excellence "Circle of Light." D.K. acknowledges funding from the Irish Research Council and the Marie Curie Actions ELEVATE fellowship. M.A. and F.-J.M.z.H. acknowledge funding from Deutsche Forschungsgemeinschaft (DFG) program SPP1391. F.-J.M.z.H. further acknowledges DFG programs SFB616 and SFB1242. B.F., S.R., and H.G. acknowledge support from DFG program SPP1391, European Research Council Advanced Grant "Complexplas," Baden-Württemberg Stiftung, German-Israeli Foundation (GIF), and Bundesministerium für Bildung, Wissenschaft, Forschung und Technologie. We acknowledge help with sample fabrication by L. Fu and H. Li. We also acknowledge the technical support by the Nano Structuring Center, Kaiserslautern.

SUPPLEMENTARY MATERIALS

www.sciencemag.org/content/355/6330/1187/suppl/DC1
Materials and Methods
Supplementary Text
Figs. S1 to S3
References (*39–46*)
Movies S1 to S3

7 September 2016; accepted 17 February 2017
10.1126/science.aaj1699

Science

Revealing the subfemtosecond dynamics of orbital angular momentum in nanoplasmonic vortices

G. Spektor, D. Kilbane, A. K. Mahro, B. Frank, S. Ristok, L. Gal, P. Kahl, D. Podbiel, S. Mathias, H. Giessen, F.-J. Meyer zu Heringdorf, M. Orenstein and M. Aeschlimann

Science **355** (6330), 1187-1191.
DOI: 10.1126/science.aaj1699

Putting plasmons in a spin

The ability of light to carry angular momentum provides an additional degree of freedom for applications such as optical tweezing and optical communication. Spektor *et al.* show that the optical angular momentum modes of light can be shrunk down to the nanometer scale through plasmonic transfer. They patterned spiral-like structures into an atomically smooth layer of gold, which allowed them to launch plasmons with controlled amounts of angular momentum.

Science, this issue p. 1187